Infectious Disease Modelling 6 (2021) 195–211

Contents lists available at ScienceDirect

Infectious Disease Modelling

journal homepage: www.keaipublishing.com/idm

Modeling the transmission of COVID-19 in the US – A case study

Chayu Yang [a], Jin Wang [b, *]

[a] Department of Mathematics, University of Florida, Gainesville, FL, 32611, USA
[b] Department of Mathematics, University of Tennessee at Chattanooga, Chattanooga, TN, 37403, USA

ARTICLE INFO

Article history:
Received 29 October 2020
Accepted 20 December 2020
Available online 30 December 2020
Handling editor: Dr. J Wu

Keywords:
COVID-19 transmission
Mathematical modeling
Data fitting

ABSTRACT

We propose a mathematical model to investigate the transmission dynamics of COVID-19. The model incorporates both human-to-human and environment-to-human transmission pathways, and employs different transmission rates to represent the epidemiological characteristics at different time periods. Using this model and publicly reported data, we perform a case study for Hamilton County, the fourth-most populous county in the state of Tennessee and a region that could represent the typical situation of COVID-19 in the United States (US). Our data fitting and simulation results show that the environment may play an important role in the transmission and spread of the coronavirus. In addition, we numerically simulate a range of epidemic scenarios and make near-term forecasts on the development and trend of COVID-19 in Hamilton County.

1. Introduction

Coronavirus disease 2019 (COVID-19) remains an on-going global pandemic at present, leading to tens of millions of cases reported in more than 210 countries and territories. The disease is caused by a novel coronavirus named severe acute respiratory syndrome coronavirus 2 (SARS-CoV-2). With the fast spread of the infection throughout the world and the high morbidity and mortality rates it causes, COVID-19 has triggered unprecedented challenges in public health and the economy. The situation is further compounded by the lack of widespread testing for COVID-19, and absence of safe vaccines and effective treatment strategies for SARS-CoV-2 (Centers for Disease Control and Prevention; WHO; World Health Organization).

Individuals infected by COVID-19 typically exhibit dry cough, fever, fatigue, and difficulty in breathing. Severe infections also lead to bilateral lung infiltration (Gralinski & Menachery, 2020). Non-respiratory symptoms such as nausea, vomiting, and diarrhea are also reported in some patients (Ellerin; Yeo, Kaushal, & Yeo, 2020; Centers for Disease Control and Prevention). The number of infections has been rapidly increasing since first reported in December 2019. Despite a large body of clinical, experimental and theoretical studies, our knowledge regarding the fundamental transmission mechanisms and the epidemiological characteristics of COVID-19 remain limited at present (Cheng & Shan, 2019; Sahin et al., 2019; Wang, 2020; Yang & Wang, 2020).

* Corresponding author.
E-mail address: Jin-Wang02@utc.edu (J. Wang).
Peer review under responsibility of KeAi Communications Co., Ltd.

https://doi.org/10.1016/j.idm.2020.12.006

Many mathematical and computational models have been proposed to quantify the transmission and spread of COVID-19 and to forecast its epidemic development. In particular, Read et al. estimated the basic reproductive number for the COVID-19 outbreak in the early stage using an assumption of Poisson-distributed daily time increments in their data fitting. Tang et al. (Tang et al., 2020) formulated a model incorporating the clinical progression of COVID-19, and found that intervention strategies such as intensive contact tracing followed by quarantine and isolation can effectively reduce the transmission risk. Imai et al., conducted computational modeling of potential epidemic trajectories in Wuhan, the first COVID-19 epicenter, and their results indicated that control measures need to block over 60% of transmission to effectively contain the outbreak. Li et al. (Li et al., 2020) applied a meta-population susceptible-exposed-infected-recovered (SEIR) model to study the epidemiological characteristics in China, and their estimates showed that a significant number of infections were undocumented. Leung et al. (Leung, Wu, Liu, & Leung, 2020) quantified the transmissibility and severity of COVID-19 and simulated the potential consequences of relaxing restrictions which could lead to a second epidemic wave.

Almost all these models are based on the SEIR compartmental framework or its variants, with a focus on the direct, human-to-human transmission pathway (Centers for Disease Control and Prevention; Chan et al., 2020; (Rothe et al., 2020); Wu, Leung, & Leung, 2020). On the other hand, the role of the environment in the transmission of COVID-19 has been largely neglected in current modeling and simulation studies (Yang & Wang, 2020; Zhong & Wang, 2020). In fact, a recent experimental study found convincing evidences that SARS-CoV-2 was detectable in aerosols for up to 3 hours, on copper for up to 4 hours, on cardboard for up to 24 hours, and on plastic and stainless steel for up to 3 days (van Doremalen et al., 2020). These findings that the virus can remain viable and infectious in aerosols and on surfaces for an extended period of time indicate a significant risk of airborne and fomite transmission for SARS-CoV-2 from the contaminated environment. For example, when infected individuals cough, sneeze or exhale, they release respiratory droplets that contain SARS-CoV-2. Most of these viral particles would fall with the droplets on nearby surfaces and objects, while others may float in the air as aerosols. Susceptible individuals could catch the coronavirus by touching the contaminated surfaces or objects and then touching their mouths, noses or eyes, or by inhaling the pathogen-laden aerosols in the air. In this pager, we will propose a new mathematical model for COVID-19 that incorporates both the human-to-human (direct) and the environment-to-human (indirect) transmission routes, with an emphasis on the role of the environment in the transmission of this disease.

Another highlight of this work is the employment of different types of transmission rates to represent the epidemiological characteristics at different time periods. Most COVID-19 epidemic models use constant transmission rates which are fixed throughout the time (see, e.g. (Imai et al., ; Leung et al., 2020; Li et al., 2020; Read et al., ; Wu et al., 2020),). In reality, however, the transmission rates may change with the epidemiological status and may be impacted by the outbreak control. For example, strong disease control measures implemented by the government such as Stay-at-Home orders, closure of schools and non-essential businesses, quarantine and isolation, and environmental sanitation and disinfection, would effectively reduce the transmission rates and minimize the transmission risk. Once such control policies are lifted, the transmission rates may quickly increase leading to high incidence and prevalence. On the other hand, when the reported infection level is high, the general public would be motivated to take voluntary action, such as wearing face masks, practicing social distancing, and washing hands often, to reduce the contact with potential infected individuals and contaminated environment and to protect themselves and their family members (Yang, Wang, Gao, & Wang, 2017). Consequently, realistic transmission rates may depend on time, disease prevalence, outbreak control and human behavior, and reflecting such features could improve the accuracy in modeling and simulating COVID-19.

As an application of our model, we study the transmission of COVID-19 in Hamilton County, the fourth-most populous county in the US state of Tennessee. Hamilton County has a total population of 367,804 (Hamilton County Health Department) and its county seat is Chattanooga, the fourth-largest city in Tennessee. In addition to Chattanooga, Hamilton County includes several small cities, towns, census-designated places and unincorporated communities, which form a region that combines both urban and rural areas. The racial makeup of the county is about 74.75% White and 25.25% other races, while on the national level the US population consists of 73.1% White Americans and 26.9% other racial groups (Wikipedia: United States..). As of September 18, 2020, there were 9,119 confirmed cases of COVID-19 in Hamilton County, with a cumulative case ratio of 2,478 per 100,000 (COVID-19 in Hamilton County ; Hamilton County Health Department), comparable to the ratio of 2,134 per 100,000 for the entire country of the US at the same time (Centers for Disease Control and Prevention). In these aspects, Hamilton County can be regarded as a place that represents the typical, or “average”, situation of COVID-19 in the US. In this study, we will fit our model to the reported data in Hamilton County to estimate key parameter values and quantify disease transmission risks at different time periods. We will also run model simulation to make near-term predictions for the epidemic development in this region.

2. Methods

We utilize a mathematical model based on differential equations to investigate the transmission dynamics of COVID-19. The model divides the host population into five classes: the susceptible individuals (denoted by S), the exposed individuals (denoted by E), the infected but non-hospitalized individuals (denoted by I), the hospitalized individuals (denoted by H), and the recovered individuals (denoted by R). Meanwhile, the model involves a compartment that represents the concentration of the coronavirus in the environment (denoted by V).

Individuals in the exposed class E are in the incubation period; they do not show symptoms, and have not been tested, but they are capable of infecting others. Individuals in the infected class I have tested positive but only show minor or moderate

symptoms; they are typically advised to self-quarantine at home and are not admitted into a hospital. Individuals in the hospitalized class H have tested positive and are at a higher risk (e.g., the elderly and those with underlying health conditions). We assume that disease induced deaths only occur in hospitalized individuals.

The following system of differential equations describes our model. Meanwhile, a flow diagram is given in Fig. 1.

$$\begin{aligned}
\frac{dS}{dt} &= \Lambda - \beta_E(I,t)SE - \beta_I(I,t)SI - \beta_H(I,t)SH - \beta_V(I,t)SV - \mu S,\\
\frac{dE}{dt} &= \beta_E(I,t)SE + \beta_I(I,t)SI + \beta_H(I,t)SH + \beta_V(I,t)SV - (\alpha+\gamma_1+\mu)E,\\
\frac{dI}{dt} &= \alpha(1-p)E - (q+\gamma_2+\mu)I,\\
\frac{dH}{dt} &= \alpha pE + qI - (w+\gamma_3+\mu)H,\\
\frac{dR}{dt} &= \gamma_1 E + \gamma_2 I + \gamma_3 H - \mu R,\\
\frac{dV}{dt} &= \xi_1 E + \xi_2 I + \xi_3 H - \sigma V.
\end{aligned} \tag{2.1}$$

The parameter Λ is the population influx rate, μ is the natural death rate for the human hosts, α^{-1} is the incubation period, p is the portion of exposed individuals who become severely ill and hospitalized after the incubation period, q is the rate of infected individuals (who initially show minor or moderate symptoms) getting hospitalized due to the worsening of their conditions, w is the disease induced death rate, σ is the removal rate of the coronavirus from the environment; γ_1, γ_2 and γ_3 are the rates of recovery, and ξ_1, ξ_2 and ξ_3 are the rates of contributing the coronavirus to the environment, from the exposed, infected (non-hospitalized), and hospitalized individuals, respectively.

We incorporate multiple transmission routes in this model, each associated with a bilinear incidence. The functions $\beta_E(I,t)$, $\beta_I(I,t)$ and $\beta_H(I,t)$ represent the direct, human-to-human transmission rates between the exposed and susceptible individuals, between the infected and susceptible individuals, and between the hospitalized and susceptible individuals, respectively, and the function $\beta_V(I,t)$ represents the indirect, environment-to-human transmission rate. In reality, since hospitalized individuals are isolated and receive intensive medical care, we may assume that they have a very low level of contact with the public (so that $\beta_H(I,t) \approx 0$) and contribute little or no pathogen to the environment (so that $\xi_3 \approx 0$). On the other hand, since self-quarantine is not strictly monitored, we assume that there is still a chance that infected individuals have contact with other people and they may also shed the coronavirus to the environment.

The values of these parameters are discussed in the Appendix, Sec. A2. Particularly, the parameters associated with the transmission rates are estimated from data fitting.

In this study, we are concerned with the application of this model to a typical place in the United States. We consider a time domain of T consecutive days, divided into three distinct intervals: $[0, T_1]$, $[T_1, T_2]$ and $[T_2, T]$, for some positive constants $0 < T_1 < T_2 < T$. The first time interval corresponds to a period when the Stay-at-Home (or, similarly, Shelter-in-Place and Safer-at-Home) orders were active so that the disease transmission rates were kept at a minimum. The second time interval is associated with a transition period when schools and businesses gradually re-opened and when the disease transmission rates would steadily increase. The third time interval is regarded as a more stabilized period, following the second, transient period, and people would have a better understanding of the disease risk and would be more rational in their behavior in order to protect themselves and their families. Particularly, when the prevalence is high, people would be more motivated to follow public health recommendations (such as wearing face masks, avoiding crowds, staying six feet apart, and washing

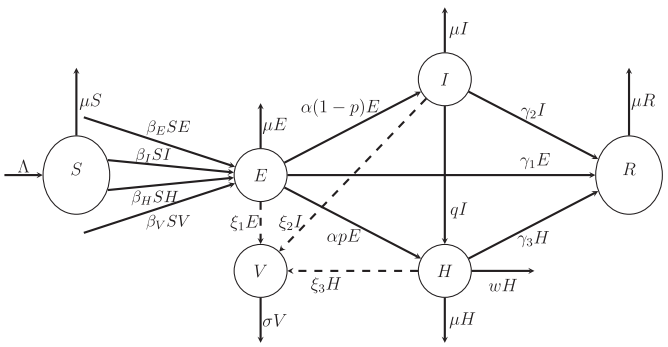

Fig. 1. A schematic representation of the model (2.1).

hands often) to reduce the chance of contracting the disease. Hence, we assume that in the third period the disease transmission rates stopped increasing monotonically but instead were shaped by the disease prevalence and human behavior.

We formulate different transmission rates in these three periods to represent their different characteristics. Per our discussion before, we assume $\beta_H(I, t) = 0$ throughout the time.

- Period 1: We assume

$$\beta_E(I,t) = \beta_{E0}, \quad \beta_I(I,t) = \beta_{I0}, \quad \beta_V(I,t) = \beta_{V0} \tag{2.2}$$

for $0 \le t \le T_1$, where β_{E0}, β_{I0} and β_{V0} are all constants, representing the minimum values of the three transmission rates because of the active Stay-at-Home order in this period. These constant transmission rates will be estimated through data fitting.

- Period 2: We assume that the three transmission rates all increase with time t in this transient period due to the re-opening of businesses, and are described by

$$\beta_E(I,t) = \beta_{E0} f(t), \quad \beta_I(I,t) = \beta_{I0} f(t), \quad \beta_V(I,t) = \beta_{V0} f(t), \tag{2.3}$$

where

$$f(t) = 1 + d(t - T_1)$$

for $T_1 \le t \le T_2$. Each transmission rate starts from its minimum at $t = T_1$ and increases monotonically with respect to t at a constant rate d. The parameter d will be determined through data fitting.

- Period 3: We assume that the three transmission rates would not monotonically increase any more; instead, they take the form

$$\beta_E(I,t) = \beta_{E0} f(T_2) g(I), \quad \beta_I(I,t) = \beta_{I0} f(T_2) g(I), \quad \beta_V(I,t) = \beta_{V0} f(T_2) g(I), \tag{2.4}$$

where $f(T_2) = 1 + d(T_2 - T_1)$, and

$$g(I) = 1 - \frac{2}{\pi} \tan^{-1}(c \cdot (I(t) - I(T_2)))$$

for $T_2 \le t \le T$. The function $g(I)$ describes the change of each transmission rate with respect to the prevalence I, due to the awareness of the infection risk by the general public and their responses to reduce the chance of contracting the pathogen. The prevalence level at the beginning of this period, $t = T_2$, is given by $I(T_2)$ and used as a reference value in this study. At any

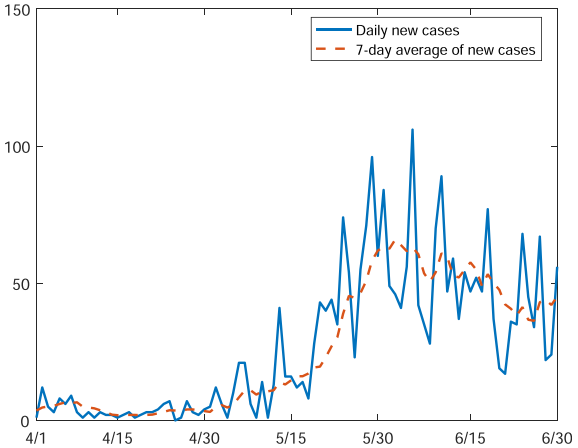

Fig. 2. Reported daily new cases and the 7-day moving average of new cases in Hamilton County from April 1 to June 30.

time t, if $I(t) > I(T_2)$, then $g(I) < 1$ and each transmission rate will be lower than its value at the point T_2. In contrast, if $I(t) < I(T_2)$, then $g(I) > 1$ and each transmission rate will be higher than its value at the point T_2. The constant c is introduced to adjust the size of the difference $I(t) - I(T_2)$, and the inverse tangent function $\tan^{-1}$ is introduced to map this difference to a standard interval $(-\pi/2, \pi/2)$. The adjustment parameter c will be determined through data fitting.

3. Results

As a case study, we apply our model to study the transmission and spread of COVID-19 in Hamilton County, located in the southeast corner of Tennessee and centered by the City of Chattanooga, with a total population of 367,804 (Hamilton County Health Department).

Fig. 2 displays the reported daily new cases and their 7-day moving average in Hamilton County for the months of April, May and June in 2020. The Stay-at-Home order in Tennessee started on April 1 and ended on April 30. As shown in Fig. 2, the number of new cases is kept at a very low level during this period, indicating a low transmission risk. Starting from April 30, there is a general trend of rapid increase for the number of new cases which lasts for about one month. This clearly marks a transient period with increasing transmission rates. After May 31, the increasing trend for the number of new cases discontinues and is replaced by an oscillatory pattern. Based on these observations, we define

- Period 1: 4/01–4/30;
- Period 2: 4/30–5/31.

In addition, we consider a relatively long time for the third period, which consists of 110 days starting from May 31; i.e.,

- Period 3: 5/31–9/18.

We then formulate different transmission rates for these three periods, as described in Section 2, and conduct data fitting and model simulation. Other parameters involved in our model and their base values are discussed in Section A2 of the Appendix.

3.1. Data fitting in Period 1

We first conduct the data fitting in Period 1 (from April 1 to April 30) to estimate the values of the parameters β_{E0}, β_{I0} and β_{V0}. Using the demographic and epidemic data reported on April 1, we set the initial condition for the host population as $(S(0), E(0), I(0), H(0), R(0)) = (367704, 50, 30, 20, 0)$ (COVID-19 in Hamilton County, ; Hamilton County Health Department). There are currently no data published for the environmental concentration of the coronavirus. To initialize V, we have tested a range of $V(0)$ and then selected $V(0) = 100$ virions/ml that yields the best fitting result.

Fig. 3 shows the numbers of cumulative confirmed cases during this period versus our fitting curve. The parameter values and their 95% confidence intervals are presented in Table 1. According to the fitted values (see Table 1), the basic reproduction number for this period is given by

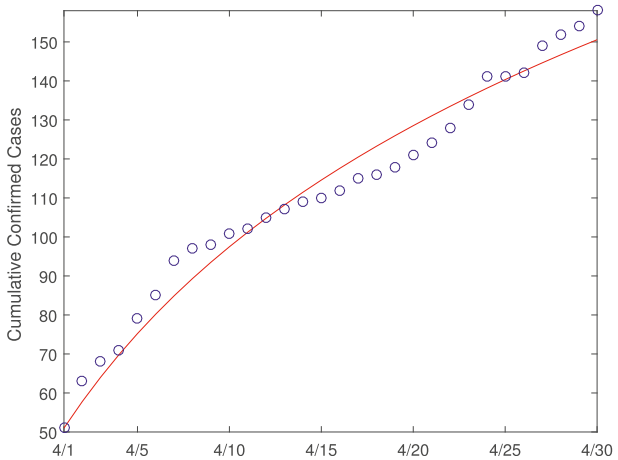

Fig. 3. Data fitting result for the cumulative confirmed cases in Hamilton County for Period 1: 4/1–4/30. The circles (in blue) denote the reported cases and the solid line (in red) denotes the fitting result.

Table 1
Parameter values estimated by curve fitting in Period 1.

Parameter	Value	Unit	95% Confidence Interval
β_{E0}	5.47×10^{-7}	person^{-1}day^{-1}	$(0, 4.67 \times 10^{-6})$
β_{I0}	2.13×10^{-8}	person^{-1}day^{-1}	$(0, 4.22 \times 10^{-6})$
β_{V0}	5.54×10^{-8}	ml $\cdot$virion^{-1}day^{-1}	$(0, 2.33 \times 10^{-6})$

$$\mathcal{R}_0 = \mathcal{R}_E + \mathcal{R}_I + \mathcal{R}_V = 0.587 + 0.036 + 0.245 = 0.868. \tag{3.1}$$

See equation (A1.3) in the Appendix for the expression of $\mathcal{R}_0$ (note that $\mathcal{R}_H = 0$). The three components $\mathcal{R}_E$, $\mathcal{R}_I$ and $\mathcal{R}_V$ represent the contributions from the three transmission routes: exposed individuals to susceptible individuals, infected individuals to susceptible individuals, and the contaminated environment to susceptible individuals, respectively. We observe that $\mathcal{R}_E$ is much higher than $\mathcal{R}_I$, indicating that the exposed individuals play a larger role than that of the infected individuals in terms of the transmission risk, since infected individuals (those who have tested positive) are generally recommended or required to self-quarantine. Meanwhile, we observe that $\mathcal{R}_V$ also contributes a significant portion to the total value of $\mathcal{R}_0$, showing the important role played by the environment-to-human transmission route. Overall, the fact that $\mathcal{R}_0 < 1$ indicates a relatively low risk of infection in Period 1, due to the active Stay-at-Home order which significantly reduces human-human and human-environment communications and effectively weakens all the transmission routes. A mathematical result concerned with this case $\mathcal{R}_0 < 1$ is stated in Theorem A3.2 in the Appendix.

To further examine the contribution of different transmission routes to the overall disease burden, we consider three sub-models associated with system (2.1) in Period 1 where all transmission rates are constants. In the first sub-model, we incorporate only the exposed-to-susceptible transmission pathway, and drop all the other transmission routes. Specifically, we modify the first two equations in system (2.1) as

$$\begin{aligned} \frac{dS}{dt} &= \Lambda - \beta_{E0} SE - \mu S, \\ \frac{dE}{dt} &= \beta_{E0} SE - (\alpha + \gamma_1 + \mu)E, \end{aligned} \tag{3.2}$$

whereas other equations in system (2.1) remain the same. Similarly, in the second sub-model, we incorporate only the infected-to-susceptible transmission pathway, with the modified equations as

$$\begin{aligned} \frac{dS}{dt} &= \Lambda - \beta_{I0} SI - \mu S, \\ \frac{dE}{dt} &= \beta_{I0} SI - (\alpha + \gamma_1 + \mu)E. \end{aligned} \tag{3.3}$$

In the third sub-model, we incorporate only the environmental-to-susceptible transmission pathway, with the modified equations as

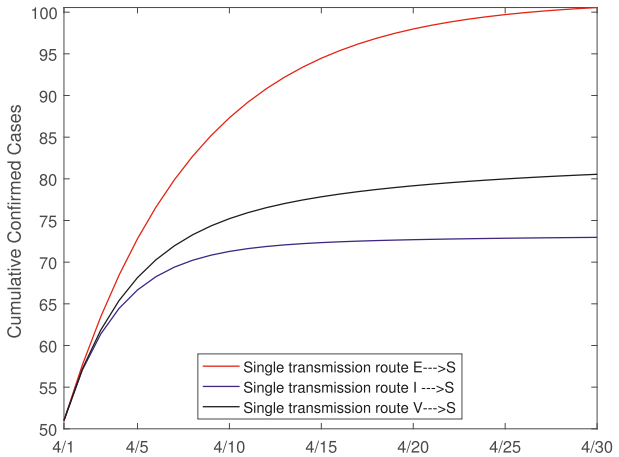

Fig. 4. Simulation result for the cumulative confirmed cases in Hamilton County during 4/1–4/30 based on three single transmission routes, represented by sub-models (3.2)–(3.4), respectively.

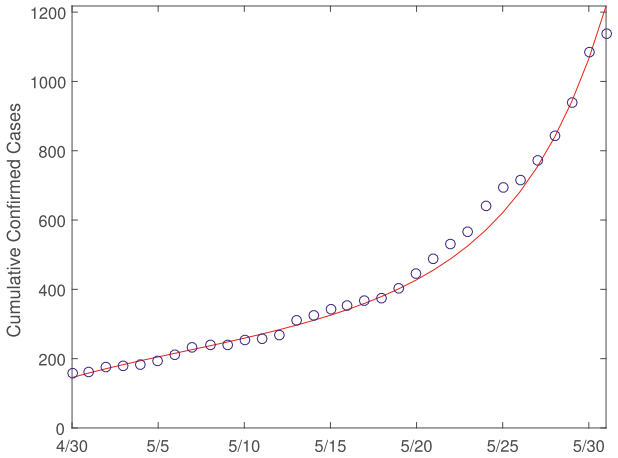

Fig. 5. Data fitting result for the cumulative confirmed cases in Hamilton County for Period 2: 4/30–5/31. The circles (in blue) denote the reported cases and the solid line (in red) denotes the fitting result.

$$\begin{aligned}\frac{dS}{dt} &= \Lambda - \beta_{V0} SV - \mu S,\\ \frac{dE}{dt} &= \beta_{V0} SV - (\alpha + \gamma_1 + \mu)E.\end{aligned} \tag{3.4}$$

We then simulate these three sub-models separately in Period 1 and plot the cumulative cases. The numerical results are presented in Fig. 4, where we observe that each transmission route generates an infection curve at a level lower than that generated by the original, multi-route model (2.1). Due to the nonlinear dynamics, the numbers represented by these three curves in Fig. 4 do not add up to the same total shown in Fig. 3. Nevertheless, it can be clearly seen that among these three transmission routes, the exposed-to-susceptible pathway generates the highest number of infections, whereas the infected-to-susceptible pathway produces the lowest number of infections. This is qualitatively consistent with the values of the reproduction numbers, shown in equation (3.1).

3.2. Data fitting in Periods 2 and 3

In Period 2, with the re-opening of businesses and schools, human activity levels gradually increased, which led to increased transmission rates, described in this work by equation (2.3). We conduct data fitting to estimate the value of the parameter d, and Fig. 5 shows the number of cumulative confirmed cases versus our fitting curve. The parameter value and its 95% confidence intervals are presented in Table 2.

In Period 3, we consider a more steady epidemic period in the sense that the transmission rates stopped their monotonic increase which took place in Period 2. A significant portion of the population followed the advice of wearing face masks and continued the practice of social distancing and personal hygiene. When disease prevalence gets higher, more people would tend to follow such disease prevention measures which would lead to decreased transmission rates. Hence, the transmission rates were shaped by the interaction between the disease prevalence and human behavior and remained as variables during Period 3, described in this work by equation (2.4).

We conduct data fitting to estimate the value of the parameter c, and Fig. 6 shows the number of cumulative confirmed cases versus our fitting curve. The parameter value and its 95% confidence intervals are presented in Table 2. Using equation (A1.3) in the Appendix and the fitted value of c (see Table 2), the basic reproduction number for Period 3 can be evaluated by

$$\mathcal{R}_0 = \mathcal{R}_E + \mathcal{R}_I + \mathcal{R}_V = 1.212 + 0.074 + 0.505 = 1.791. \tag{3.5}$$

Note also that $\mathcal{R}_H = 0$. Compared to the reproduction numbers in Period 1, given in equation (3.1), we see a similar pattern: the exposed-to-susceptible and infected-to-susceptible transmission routes make the highest and lowest contributions, respectively, and the environment-to-human transmission pathway plays an important role, toward shaping the overall disease risk. The difference, however, is that all the values of $\mathcal{R}_E$, $\mathcal{R}_I$ and $\mathcal{R}_V$ are significantly increased, leading to the total $\mathcal{R}_0 > 1$ in Period 3 and indicating the persistence of the disease. A mathematical description of this result is provided by Theorem A3.2 in the Appendix.

Table 2
Parameter values estimated by curve fitting in Periods 2 and 3.

Parameter	Value	Unit	95% Confidence Interval
d (Period 2)	3.76×10^{-2}	day^{-1}	$(3.70 \times 10^{-2}, 3.83 \times 10^{-2})$
c (Period 3)	4.70×10^{-3}	person^{-1}	$(4.36 \times 10^{-3}, 5.05 \times 10^{-3})$

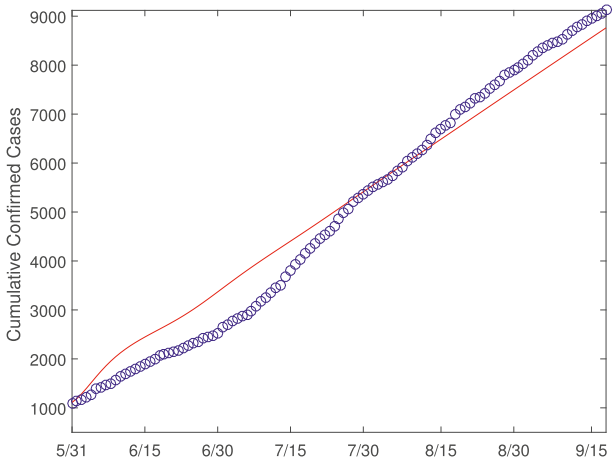

Fig. 6. Data fitting result for the cumulative confirmed cases in Hamilton County for Period 3: 5/31–9/18. The circles (in blue) denote the reported cases and the solid line (in red) denotes the fitting result.

Table 3
Parameter values estimated by curve fitting in the entire time domain.

Parameter	Value	Unit	95% Confidence Interval
β_{E0}	7.38×10^{-7}	$\text{person}^{-1}\text{day}^{-1}$	$(6.35 \times 10^{-7}, 8.41 \times 10^{-7})$
β_{I0}	5.61×10^{-10}	$\text{person}^{-1}\text{day}^{-1}$	$(0, 6.68 \times 10^{-8})$
β_{V0}	7.38×10^{-8}	$\text{ml} \cdot \text{virion}^{-1}\text{day}^{-1}$	$(6.70 \times 10^{-8}, 8.02 \times 10^{-8})$

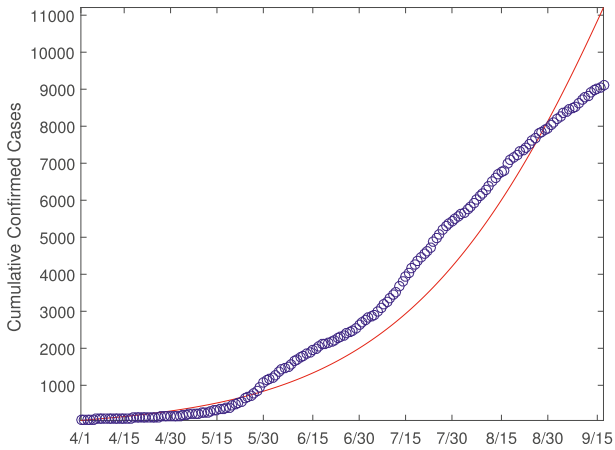

Fig. 7. Data fitting result for the cumulative confirmed cases in Hamilton County for the entire time domain (4/1–9/18) based on uniform, constant transmission rates. The circles (in blue) denote the reported cases and the solid line (in red) denotes the fitting result.

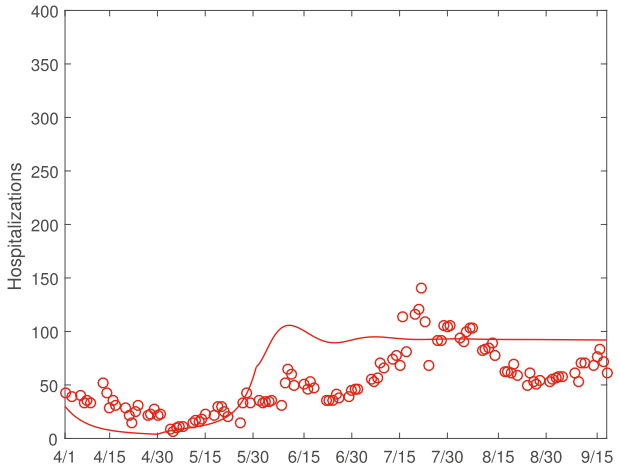

Fig. 8. Comparison between the reported number of hospitalized individuals and the numerical simulation result. The circles represent the reported cases and the solid line represents the simulation result.

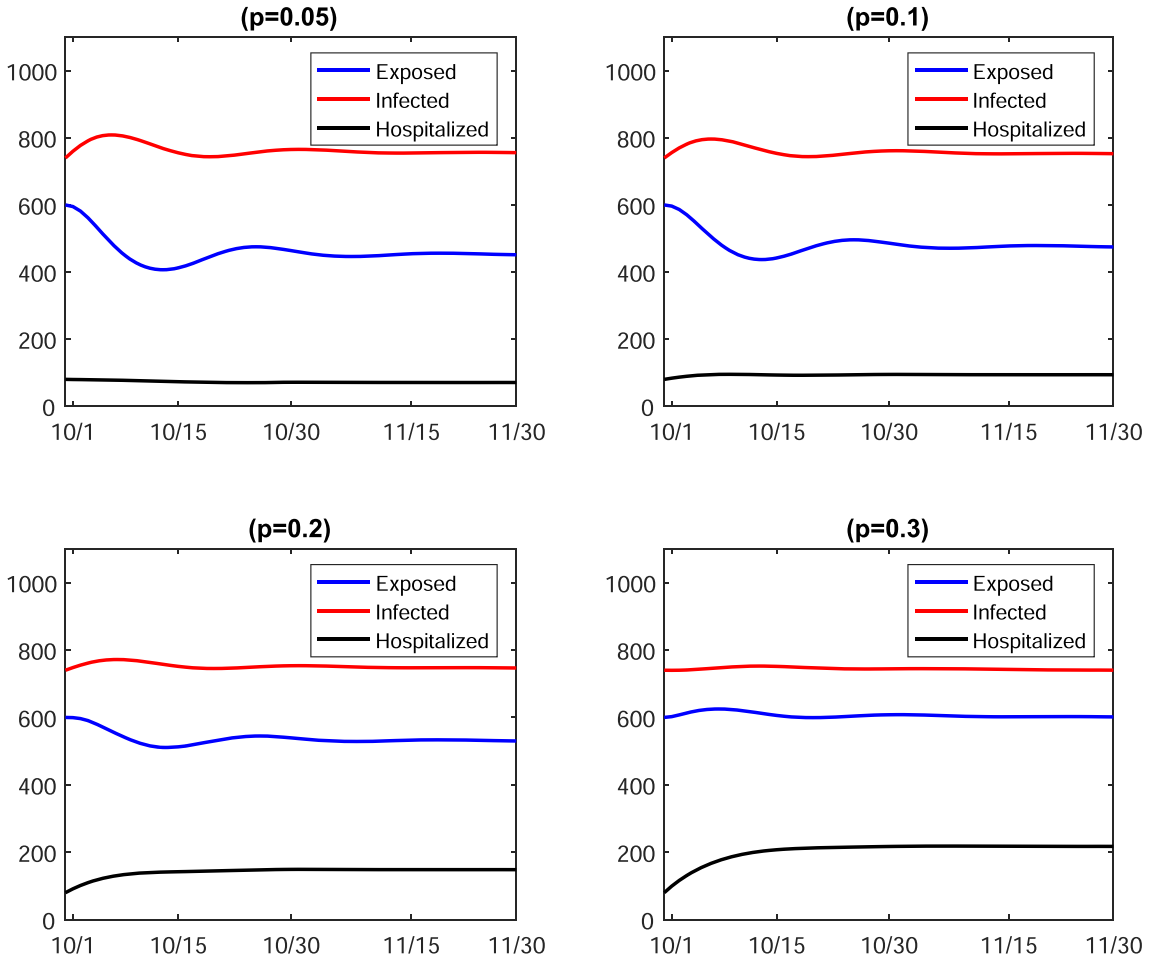

Fig. 9. Simulation results for the numbers of the exposed, infected and hospitalized individuals from 10/1 to 11/30, with different values of the hospitalization rate p due to severe infections.

Our numerical study and data fitting involve three time periods employing different representations of the transmission rates. For comparison, we have also conducted data fitting for the model (2.1) using uniform, constant transmission rates throughout all the three periods. The values of the parameters (i.e., the constant transmission rates β_{E0}, β_{I0} and β_{V0}) estimated from the fitting are provided in Table 3. Meanwhile, Fig. 7 shows the fitting result for the cumulative cases.

To measure and compare the goodness-of-fit, we calculate the normalized root-mean-square error (NRMSE) for each approach. The NRMSE is generally defined as follows:

$$\text{NRMSE} = \frac{\sqrt{n\sum_{i=1}^{n}(y_i - x_i)^2}}{\sum_{i=1}^{n} x_i},$$

where $x_i\,(1 \le i \le n)$ are reported data, $y_i\,(1 \le i \le n)$ are computed data, and n is the number of data points used. For the entire duration from 4/1 to 9/18, We found that the NRMSE is 0.12 based on our approach of using different, time-dependent transmission rates on the three time periods, and the NRMSE is 0.22 by using uniform, constant transmission rates for all the three periods. This is a demonstration that our proposed approach has a better performance in fitting the data than that based on the standard practice of using constant transmission rates.

One of the major concerns of the health administrations in almost every place is whether the hospital capacity can meet the demands of COVID-19 patients. A mathematical model can provide useful insight in simulating and predicting hospital needs. Based on our model (2.1) and data fitting results for Hamilton County, we have also conducted numerical simulation to the number of hospitalized individuals, represented by H in our model, and compared with the reported hospitalized cases from April 1 to September 18. Fig. 8 displays the result.

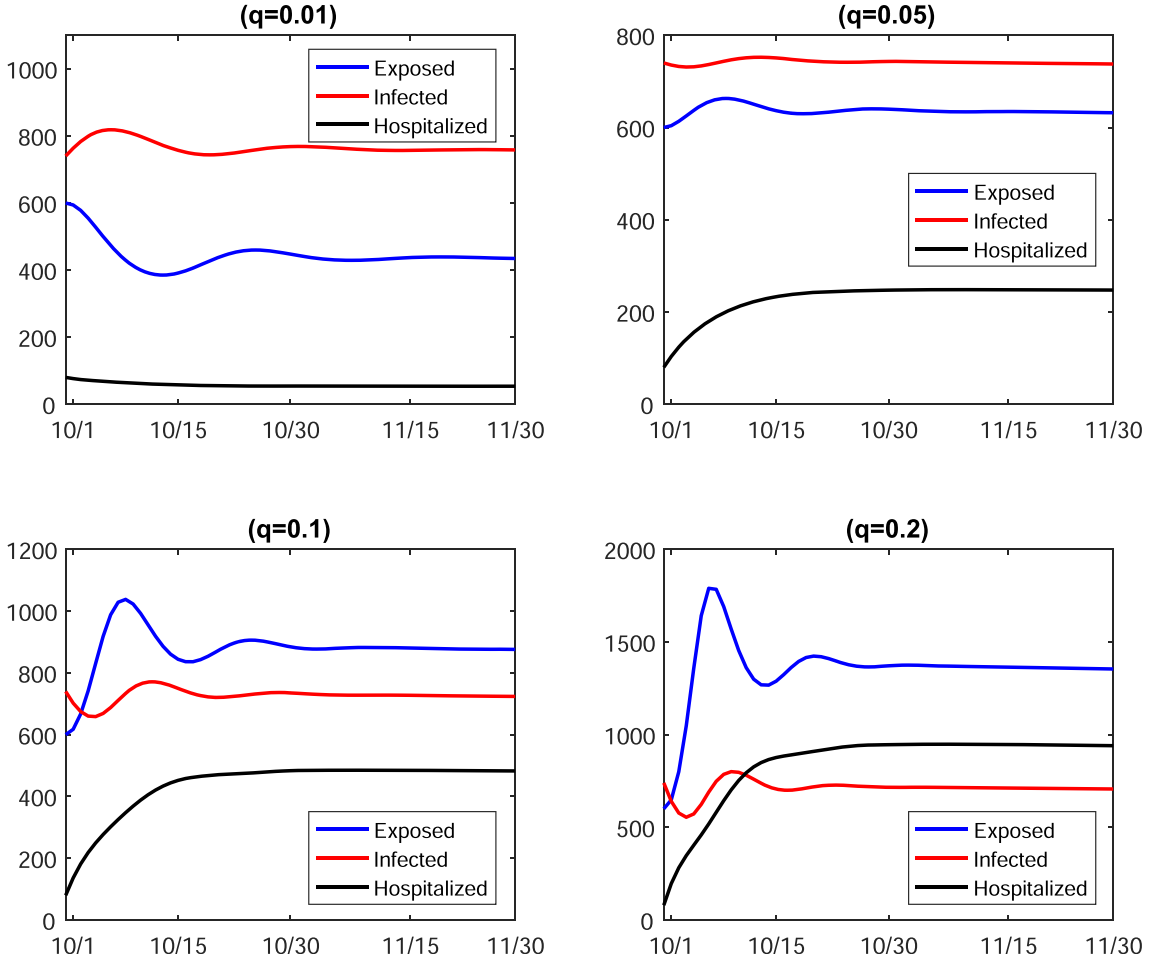

Fig. 10. Simulation results for the numbers of the exposed, infected and hospitalized individuals from 10/1 to 11/30, with different values of the hospitalization rate q due to minor or moderate infections.

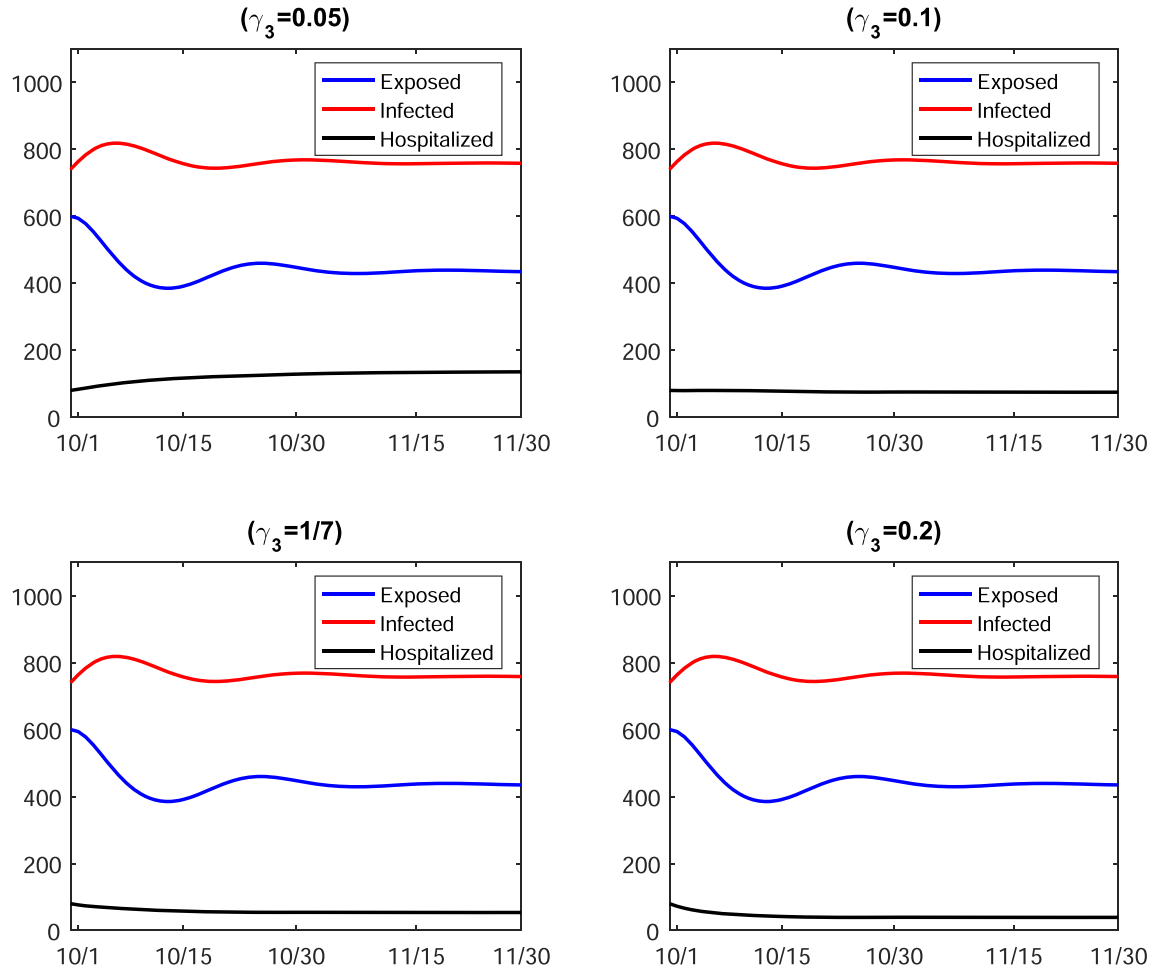

Fig. 11. Simulation results for the numbers of the exposed, infected and hospitalized individuals from 10/1 to 11/30, with different lengths of the average hospital stay represented by $1/\gamma_3$.

3.3. Simulation results with varied parameters

Using the parameter values estimated through data fitting, we can make simulation and prediction for the COVID-19 epidemic development in Hamilton County for the near future by running the model (2.1). Meanwhile, we have also considered the variation of several important model parameters. The values of the model parameters could be impacted by a number of factors, including the change of environmental conditions (such as temperature and rainfall), change of the economic situation and health care standards in the region, evolution of the immunity level in the host population, mutation of the viral strains, and availability of new therapeutic treatment. Though, many of such changes will probably only happen in the long term.

Fig. 9 shows the simulation results on the evolution of the numbers of the exposed, infected and hospitalized individuals from October 1 to November 30, with different hospitalization rate p due to severe infections. The base value is $p = 0.1$ (i.e., 10%) in our model. This value, however, possibly varies with time. In Fig. 9 we present simulation results with 4 different values of the hospitalization rate related to severe infections: $p = 0.05$, 0.1, 0.2 and 0.3, while other parameters remain fixed. As can be naturally expected, a higher value of p leads to a larger number of hospitalized individuals. Though, the increase of hospitalized cases appears gradual and smooth, and the simulation does not show any surge of hospitalized COVID-19 patients during this two-month period. On the other hand, the impact of the variation in p on the numbers of exposed and infected individuals seems to be minor during this period.

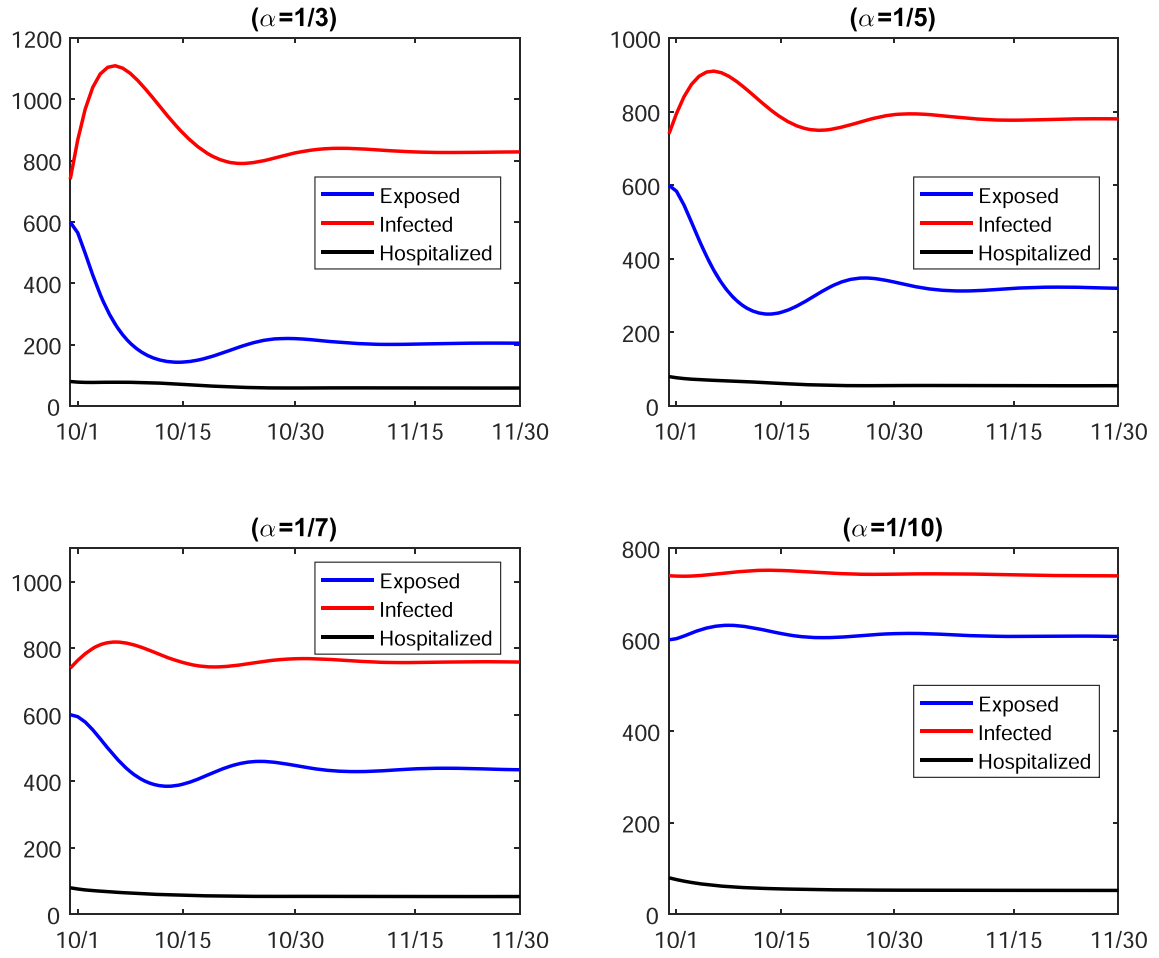

Fig. 12. Simulation results for the numbers of the exposed, infected and hospitalized individuals from 10/1 to 11/30, with different lengths of the average incubation period represented by $1/\alpha$.

Fig. 10 shows our simulation results for the exposed, infected and hospitalized populations from October 1 to November 30, when the hospitalization rate q related to minor or moderate infections varies. We have assumed that among individuals with non-severe infections (who are classified into the I class in our model), a small portion may be later admitted into a hospital for reasons such as an exacerbation of health conditions. The base value is $q = 0.01$ in our model. In Fig. 10 we explore the possible scenarios with 4 different values for this parameter: $q = 0.01$, 0.05, 0.1 and 0.2, while other parameters remain fixed. We observe that the value of q seems to have a more significant impact than that of p on the hospitalized cases. In particular, when $q = 0.1$ and $q = 0.2$, the number of hospitalized individuals rises rapidly to 500 and 1,000, respectively. Meanwhile, with a higher value of q, the level of I decreases accordingly, since more individuals move from the infected class I to the hospitalized class H.

Fig. 11 illustrates the impact of the length of hospital stays in this two-month period. The parameter γ_3 in our model represents the reciprocal of the average hospital duration, and its base value is $\gamma_3 = 1/7$. We simulate the evolution of the exposed, infected and hospitalized populations in Fig. 11 at 4 different values: $\gamma_3 = 0.05$, 0.1, 1/7 and 0.2, with other parameters fixed at their base values. A smaller value of γ_3 corresponds to a longer hospital stay in average, which leads to a higher number of hospitalized patients at a time. In particular, we observe that the hospitalized cases gradually increase to 200 when $\gamma_3 = 0.05$, whereas the numbers remain below 100 when $\gamma_3 = 1/7$ and 1/5.

In addition, we have also considered the impact of the incubation period on the epidemic development. The parameter α in our model represents the reciprocal of the average incubation length, and its base value is $\alpha = 1/7$. Fig. 12 shows the simulation results with 4 different values: $\alpha = 1/3$, 1/5, 1/7 and 1/10, while other parameters are fixed. We observe that the

variation of α changes the hospitalized number H very little, however it has a significant impact on the infected number I. A larger value of α corresponds to a shorter incubation period, which then leads to a higher level of infected cases I at a time. In particular, when $\alpha = 1/3$, the infection level could reach as high as 1,100, compared to 800 at the base value $\alpha = 1/7$.

4. Discussion

We have presented a new mathematical model to investigate the transmission dynamics of COVID-19. The model incorporates multiple transmission routes that include both human-to-human and environment-to-human pathways. Our modeling study is conducted by dividing the time domain into three distinct periods: the first period with an active Stay-at-Home order, the second period with a transient increase of disease incidence and prevalence, and the third period with a more stabilized epidemic development. We then formulate different types of transmission rates to represent the characteristic of these three different periods: constant transmission rates that reflect the minimum incidence in Period 1, variable transmission rates that increase monotonically with time in Period 2, and variable transmission rates that are shaped by the disease prevalence and human behavior in Period 3.

As a case study, we have applied our model to Hamilton County in the US state of Tennessee. Results show that our data fitting approach based on different transmission rates in different time periods has a better performance than that based on the standard approach of using uniform, constant transmission rates throughout the entire time domain. Results also indicate that the environment may play an important role in the transmission and spread of COVID-19. In addition, we have conducted numerical simulation to make near-term predictions for the epidemic development in Hamilton County, with the variation of several important model parameters that could represent a range of epidemic scenarios.

Our simulation results show that under most of these parameter settings, there would be no surge on the numbers of the infected and hospitalized individuals, indicating that the second wave of COVID-19 is not likely to take place in Hamilton County in the short term (until November 30). An exception may occur if the hospitalization rate related to minor/moderate disease symptoms becomes very large, for reasons such as a mutation of the coronavirus with a significantly different infection mechanism. This could cause the number of hospitalized patients to rapidly increase to a level as high as 1,000 (shown in Fig. 10) which would well exceed the hospital capacity in Hamilton County (COVID-19 in Hamilton County, ; Hamilton County Health Department), though the chance for this to happen is considered low. Another scenario which may largely impact the epidemic development in this region is a significant reduction of the length of the incubation period. When the average incubation period becomes as short as 3 days, the number of infected individuals could rise to a peak of 1,100 (see Fig. 12), in contrast to a level of 800 under other parameter settings. This may also be caused, though with a low probability, a mutation of the viral strains.

There are, however, several limitations in this study. Our model has not considered the impact of the age distribution of the host population, whereas COVID-19 infections exhibit significant differences in risk factors, disease severity and mortality rates among different age groups (with the elderly being the most vulnerable) (Centers for Disease Control and Prevention; World Health Organization). The model can be extended to explicitly incorporate the age structure of the hosts, with age-dependent parameters such as the transmission rates, hospitalization rates, and incubation and recovery periods. Meanwhile, our model application has not considered the long-term evolution of COVID-19 in Hamilton County, and the simulation results may not reflect the situation in the distant future as the epidemic and pandemic characteristics might undergo significant changes in the long run. In addition, the quality of our data fitting may be impacted by the fact that there are currently no published data on the environmental concentration and distribution of the coronavirus. We hope to be able to improve this modeling study when such data are available.

Declaration of competing interest

Both authors, Chayu Yang and Jin Wang, declare that there is no conflict of interest in this work.

Acknowledgments

The authors would like to thank Greg Heath, Jesse Houser and Charlie Mix for providing data resources related to COVID-19 in Hamilton County. This work was partially supported by the National Institutes of Health under grant number 1R15GM131315.

Appendix

A1. Basic reproduction number

In the first and third time periods, the model (2.1) is an autonomous dynamical system and the transmission rates are either constants (including 0), or functions of I only. They can be generally represented as $\beta_E(I, t) = \beta_E(I)$, $\beta_I(I, t) = \beta_I(I)$, $\beta_H(I, t) = \beta_H(I)$, and $\beta_V(I, t) = \beta_V(I)$, for $0 \le t \le T_1$ or $T_2 \le t \le T$. For such an autonomous system, the basic reproduction number can be computed using the standard next-generation matrix technique (van den Driessche & Watmough, 2002).

Apparently, system (2.1) has a unique disease-free equilibrium (DFE) at

$$X_0 = (S_0, E_0, I_0, H_0, R_0, V_0) = \left(\frac{\Lambda}{\mu}, 0, 0, 0, 0, 0\right) \tag{A1.1}$$

We treat E, I, H and V as the infection components in our model, thus the new infection matrix F and the transition matrix V are given by

$$F = \begin{bmatrix} \beta_E(0)S_0 & \beta_I(0)S_0 & \beta_H(0)S_0 & \beta_V(0)S_0 \\ 0 & 0 & 0 & 0 \\ 0 & 0 & 0 & 0 \\ 0 & 0 & 0 & 0 \end{bmatrix}, \quad V = \begin{bmatrix} u_1 & 0 & 0 & 0 \\ -\alpha(1-p) & u_2 & 0 & 0 \\ -\alpha p & -q & u_3 & 0 \\ -\xi_1 & -\xi_2 & -\xi_3 & \sigma \end{bmatrix}, \tag{A1.2}$$

where $u_1 = \alpha + \gamma_1 + \mu$, $u_2 = q + \gamma_2 + \mu$, and $u_3 = w + \gamma_3 + \mu$. The basic reproduction number of model (2.1) is then defined as the spectral radius of the next generation matrix FV^{-1}; i.e.,

$$\mathcal{R}_0 = \rho(FV^{-1}) = \mathcal{R}_E + \mathcal{R}_I + \mathcal{R}_H + \mathcal{R}_V, \tag{A1.3}$$

where

$$\begin{aligned} \mathcal{R}_E &= \frac{\beta_E(0)S_0}{u_1}, \\ \mathcal{R}_I &= \frac{\alpha(1-p)\beta_I(0)S_0}{u_1 u_2}, \\ \mathcal{R}_H &= \frac{\alpha\beta_H(0)S_0}{u_1 u_3}\left(p + \frac{q(1-p)}{u_2}\right), \\ \mathcal{R}_V &= \frac{\beta_V(0)S_0}{\sigma u_1}\left(\xi_1 + \frac{\xi_2\alpha(1-p)}{u_2} + \frac{\xi_3\alpha}{u_3}\left(p + \frac{q(1-p)}{u_2}\right)\right), \end{aligned}$$

which provides a measurement for the disease risk during Period 1 and Period 3. The first three terms $\mathcal{R}_E$, $\mathcal{R}_I$ and $\mathcal{R}_H$ characterize the contribution of the three human-to-human transmission routes originated from the exposed, infected and hospitalized individuals, respectively, and the fourth term $\mathcal{R}_V$ characterize the contribution from the environment-to-human transmission route.

A2. Parameter values

We obtain the values of the model parameters from the literature and through data fitting. The incubation period of the infection ranges between 2 and 14 days, with a mean of 5–7 days (Spencer et al.,); we take the base value of $\alpha^{-1} = 7$ days in our model. Recovery from COVID-19 has a wide variation (1.5–30 days) among different patients (Spencer et al.,; Centers for Disease Control and Prevention; World Health Organization; WHO), depending on their severity, age and overall health. In our model, disease recovery occurs in exposed, infected and hospitalized individuals. Those recover directly from the exposed state typically exhibit no symptoms and have a fast recovery; we set their average recovery period as 5 days in our model, which leads to $\gamma_1 = 1/5$ per day. The majority of the infected individuals, with minor or moderate symptoms, may recover without going to a hospital; we set their average recovery period as 14 days, which leads to $\gamma_1 = 1/14$ per day. The hospitalized individuals, though typically with more severe conditions, receive intensive medical treatment which may help them to recover faster than those who are not admitted into a hospital; we set their average recovery period as 7 days, which leads to $\gamma_3 = 1/7$ per day. Members of the coronavirus family can survive in the environment from a few hours to several days (Geller, Varbanov, & Duval, 2012; (Kampf et al., 2020); van Doremalen et al., 2020) and we take the value of 2 days, which results in a virus removal rate $\sigma = 1/2$ per day. We assume that the population migration rates into and out of the region are the same so that we may express the influx rate of susceptible individuals as $\Lambda = \mu N$, where N is the size of the total population in the region. Since the time period in our study is relatively short, we also assume that the natural birth and death rates are both equal to μ. We take the values of virus shedding rates for exposed and infected individuals from (Yang & Wang, 2020). Since hospitalized individuals are strictly isolated, we assume that the virus shedding rate from the hospitalized individuals to the environment is zero; i.e., $\xi_3 = 0$. Among individuals who have tested positive, the portion of severe infections (which would lead to hospital admission) ranges from 5% to 20% (WHO), and we take the base value of $p = 10\%$ in our model. Meanwhile, we assume that among those infected individuals with minor or moderate symptoms, a very small portion q would require hospital care at some point and we take the base value of $q = 0.01$ in this study. Other parameter values, especially those related to the transmission rates, are determined through model fitting based on the reported data in Hamilton County (COVID-19 in Hamilton County,).

Table A1
Model parameters and their base values (p = person, d = day)

Parameter	Description	Value	Source
N	Population size in Hamilton County	367804 p	(Data USA,)
μ	Natural birth and death rate	2.74×10^{-5}/d	(Hamilton County Health Department)
α	Reciprocal of the incubation period	1/7/d	Spencer et al.
w	Disease-induced death rate	0.01/d	World Health Organization,
σ	Environmental removal rate of virus	0.5/d	van Doremalen et al. (2020)
γ_1	Recovery rate of exposed individuals	1/5/d	WHO,
γ_2	Recovery rate of infected individuals	1/14/d	WHO,
γ_3	Recovery rate of hospitalized individuals	1/7/d	Spencer et al.
ξ_1	Virus shedding rate by exposed individuals	2.3/ml/p/d	Yang and Wang (2020)
ξ_2	Virus shedding rate by infected individuals	1.15/ml/p/d	Yang and Wang (2020)
ξ_3	Virus shedding rate by hospitalized individuals	0	Assumed
p	Rate of hospitalization due to severe infections	10%	WHO,
q	Rate of hospitalization due to minor infections	0.01/d	Assumed
β_E	Transmission rate between classes S and E	fitting by data	–
β_I	Transmission rate between classes S and I	fitting by data	–
β_V	Transmission rate between classes S and V	fitting by data	–
β_H	Transmission rate between classes S and H	0	Assumed

A3. Equilibrium analysis

When the model (2.1) is an autonomous system (in Period 1 and Period 3), we are able to conduct a detailed equilibrium analysis to investigate its main dynamical properties. Let (S, E, I, H, R, V) be an equilibrium of system (2.1). By solving the following system

$$\begin{cases} \Lambda - \beta_E(I)SE - \beta_I(I)SI - \beta_H(I)SH - \beta_V(I)SV - \mu S = 0, \\ \beta_E(I)SE + \beta_I(I)SI + \beta_H(I)SH + \beta_V(I)SV - (\alpha + \gamma_1 + \mu)E = 0, \\ \alpha(1-p)E - (q + \gamma_2 + \mu)I = 0, \\ \alpha pE + qI - (w + \gamma_3 + \mu)H = 0, \\ \gamma_1 E + \gamma_2 I + \gamma_3 H - \mu R = 0, \\ \xi_1 E + \xi_2 I + \xi_3 H - \sigma V = 0, \end{cases} \tag{A3.1}$$

one can verify that there is a unique positive endemic equilibrium (EE)

$$X_* = (S_*, E_*, I_*, H_*, R_*, V_*)$$

if and only if $\mathcal{R}_0 > 1$, where $S_* = \frac{S_0}{\mathcal{R}_0}$, $E_* = \frac{\Lambda - \mu S_*}{u_1}$, $I_* = \frac{\alpha(1-p)E_*}{u_2}$, $H_* = \frac{\alpha p E_* + qI_*}{u_3}$, and $V_* = \frac{\xi_1 E_* + \xi_2 I_*}{\sigma}$. Thus, we have

Theorem A3.1. *System (2.1) has at most two equilibria, the DFE and EE.*

(1) *If $\mathcal{R}_0 \le 1$, the DEF X_0 is the only equilibrium for the model (2.1).*
(2) *If $\mathcal{R}_0 > 1$, the model (2.1) admits two equilibria, the DEF X_0 and the EE X_*.*

In what follows, we perform a study on the global stability of the DFE. By a simple comparison principle, we can assume that $0 \le S + E + I + H + R \le S_0$, $0 \le V \le \frac{\xi S_0}{\sigma}$, where $\xi = \max\{\xi_1, \xi_2, \xi_3\}$ and the biologically feasible domain is given by

$$\Omega = \left\{ \left(S, E, I, H, R, V\right) \in \mathbb{R}^5_+ : S + E + I + H + R \le S_0,\ 0 \le V \le \frac{\xi S_0}{\sigma} \right\}$$

Theorem A3.2. *The following statements hold for the model (2.1).*

(1) If $\mathcal{R}_0 \le 1$, the DFE of system (2.1) is globally asymptotically stable in Ω.
(2) If $\mathcal{R}_0 > 1$, the DFE of system (2.1) is unstable and there exists a unique endemic equilibrium. Moreover, the disease is uniformly persistent in the interior of Ω, denoted by Ω; namely, $\liminf_{t\to\infty} (E(t), I(t), H(t), V(t)) > (\epsilon, \epsilon, \epsilon, \epsilon)$ for some $\epsilon > 0$.

Proof. Let $\mathbf{X} = (E,I,H,V)^T$. One can verify that

$$\frac{d\mathbf{X}}{dt} \le (F - V)\mathbf{X},$$

where the matrices F and V are given in equation (A1.2). By some algebraic manipulation, we let $\mathbf{u} = (\beta_E, \beta_I, \beta_H, \beta_V)$. It then follows from the fact $\mathcal{R}_0 = \rho(FV^{-1}) = \rho(V^{-1}F)$ and direct calculation that $\mathbf{u}$ is a left eigenvector associated with the eigenvalue $\mathcal{R}_0$ of the matrix $V-^1F$; i.e., $\mathbf{u}V^{-1}F = \mathcal{R}_0\mathbf{u}$. Consider a Lyapunov function

$$\mathcal{L}_0 = \mathbf{u}V^{-1}\mathbf{X}.$$

Differentiating $\mathcal{L}$ along the solutions of (2.1), we have

$$\frac{d\mathcal{L}_0}{dt} = \mathbf{u}V^{-1}\frac{d\mathbf{X}}{dt} \leq \mathbf{u}V^{-1}(F-V)\mathbf{X} = \mathbf{u}(\mathcal{R}_0 - 1)\mathbf{X}. \tag{A3.2}$$

If $\mathcal{R}_0 < 1$, the equality $\frac{d\mathcal{L}_0}{dt} = 0$ implies that $\mathbf{u}\mathbf{X} = 0$. This leads to $E = I = H = V = 0$ by noting that all components of $\mathbf{u}$ are positive. Hence, when $\mathcal{R}_0 < 1$, equations of (A3.1) yield $S = S_0$, and $E = I = H = R = V = 0$. Thus, the invariant set on which $\frac{d\mathcal{L}_0}{dt} = 0$ contains only the point X_0.

If $\mathcal{R}_0 = 1$, then the equality $\frac{d\mathcal{L}_0}{dt} = 0$ implies that

$$\left(\frac{\beta_E S}{S_0} + \frac{u_1\mathcal{R}_I}{S_0} + \frac{u_1\mathcal{R}_H}{S_0} + \frac{u_1\mathcal{R}_V}{S_0} - \frac{u_1}{S_0}\right)E + \left(\frac{S}{S_0} - 1\right)\left(\beta_I I + \beta_H H + \beta_V V\right) = 0.$$

Obviously, $\frac{S}{S_0} - 1 \leq 0$ and

$$\frac{\beta_E S}{S_0} + \frac{u_1\mathcal{R}_I}{S_0} + \frac{u_1\mathcal{R}_H}{S_0} + \frac{u_1\mathcal{R}_V}{S_0} - \frac{u_1}{S_0} \leq \frac{u_1}{S_0}(\mathcal{R}_0 - 1) = 0.$$

Hence, we have either $E = I = H = V = 0$, or $S = S_0$. As analyzed before, each case would indicate that the DEF X_0 is the only invariant set on $\{(S,E,I,H,R,V) \in \Omega : \frac{d\mathcal{L}_0}{dt} = 0\}$.

Therefore, when $\mathcal{R}_0 < 1$ or $\mathcal{R}_0 = 1$, the largest invariant set on which $\frac{d\mathcal{L}_0}{dt} = 0$ consists of the singleton $X_0 = (S_0, 0, 0, 0, 0)$. By LaSalle's Invariance Principle (LaSalle, 1976), the DFE is globally asymptotically stable in Ω if $\mathcal{R}_0 \leq 1$.

In contrast, if $\mathcal{R}_0 > 1$, then it follows from the continuity of vector fields that $\frac{d\mathcal{L}_0}{dt} > 0$ in a neighborhood of the DFE in Ω. Thus the DFE is unstable by the Lyapunov stability theory. □

Theorem A3.2 shows that the disease will be eliminated if $\mathcal{R}_0 \leq 1$, whereas the infection will persist if $\mathcal{R}_0 > 1$. The results underscore the importance of reducing $\mathcal{R}_0$ below unity in order to contain and eventually eradicate the disease. The condition $\mathcal{R}_0 \leq 1$ could be achieved through effective public health policies and outbreak intervention strategies, and through the control of both the direct and indirect transmission routes.

References

Centers for Disease Control and Prevention: Coronavirus (COVID-19). Available at: https://www.cdc.gov/coronavirus/2019-ncov.

Chan, J. F.-W., Yuan, S., Kok, K.-H., et al. (2020). A familial cluster of pneumonia associated with the 2019 novel coronavirus indicating person-to-person transmission: A study of a family cluster. *Lancet, 395*, 514–523.

Cheng, Z. J., & Shan, J. (2019). Novel coronavirus: Where we are and what we know. *Infection, 48*, 155–163, 2020.

COVID-19 in Hamilton County, TN. Available at: https://sites.google.com/view/hamiltoncounty-tn-covid19.

Data USA: Chattanooga, TN. Available at: https://datausa.io/profile/geo/chattanooga-tn/.

van Doremalen, N., Bushmaker, T., Morris, D. H., et al. (2020). Aerosol and surface stability of SARS-CoV-2 as compared with SARS-CoV-1. *New England Journal of Medicine, 382*, 1564–1567.

van den Driessche, P., & Watmough, J. (2002). Reproduction numbers and sub-threshold endemic equilibria for compartmental models of disease transmission. *Mathematical Biosciences, 180*, 29–48.

Ellerin, T. (January 2020). The new coronavirus: What we do - and don't - know. *Harvard Health Blog, 25*. Available at: https://www.health.harvard.edu/blog/the-new-coronavirus-what-we-do-and-dont-know-2020012518747.

Geller, C., Varbanov, M., & Duval, R. E. (2012). Human coronaviruses: Insights into environmental resistance and its influence on the development of new antiseptic strategies. *Viruses, 4*(11), 3044–3068.

Gralinski, L. E., & Menachery, V. D. (2020). Return of the Coronavirus: 2019-nCoV. *Viruses, 12*(2), 135.

Hamilton County Health Department. Available at: http://health.hamiltontn.org.

N. Imai, A. Cori, I. Dorigatti, M. Baguelin, C.A. Donnelly, S. Riley, et al, Report 3: Transmissibility of 2019-nCoV, published online January 25, 2020. Available at: https://www.imperial.ac.uk/mrc-global-infectious-disease-analysis/news–wuhan-coronavirus/.

Kampf, G., Todt, D., Pfaender, S., & Steinmann, E. (2020). Persistence of coronaviruses on inanimate surfaces and its inactivation with biocidal agents. *Journal of Hospital Infection, 104*(3), 246–251.

LaSalle, J. P. (1976). *The stability of dynamical systems, regional conference series in applied mathematics*. Philadelphia: SIAM.

Leung, K., Wu, J. T., Liu, D., & Leung, G. M. (2020). First-wave COVID-19 transmissibility and severity in China outside Hubei after control measures, and second-wave scenario planning: A modelling impact assessment. *Lancet, 395*, 1382–1393.

Li, R., Pei, S., Chen, B., Song, Y., Zhang, T., Yang, W., et al. (2020). Substantial undocumented infection facilitates the rapid dissemination of novel coronavirus (SARS-CoV2). *Science, 368*, 489–493.

J.M. Read, J.R.E. Bridgen, D.A.T. Cummings, A. Ho and C.P. Jewell, Novel coronavirus 2019-nCoV: early estimation of epidemiological parameters and epidemic predictions, available at: medRxiv. DOI: https://doi.org/10.1101/2020.01.23.20018549.

Rothe, C., Schunk, M., Sothmann, P., et al. (2020). Transmission of 2019-nCoV infection from an asymptomatic contact in Germany. *New England Journal of Medicine, 382*, 970–971.

Sahin, A., Erdogan, A., Agaoglu, P. M., Dineri, Y., Cakirci, A., Senel, M., et al. (2019). Novel coronavirus (COVID-19) outbreak: A review of the current literature. *Eurasian Journal of Medicine and Oncology, 4*(1), 1–7, 2020.

J.A. Spencer, D.P. Shutt, S.K. Moser, H. Clegg, H.J. Wearing, H. Mukundan, and C.A. Manore, Epidemiological parameter review and comparative dynamics of influenza, respiratory syncytial virus, rhinovirus, human coronavirus, and adenovirus. DOI: https://doi.org/10.1101/2020.02.04.20020404.
Tang, B., Wang, X., Li, Q., Bragazzi, N. L., Tang, S., Xiao, Y., et al. (2020). Estimation of the transmission risk of 2019-nCoV and its implication for public health interventions. *Journal of Clinical Medicine, 9*(2), 462.
Wang, J. (2020). Mathematical models for COVID-19: Applications, limitations, and potentials. *Journal of Public Health and Emergency, 4*(9).
WHO Coronavirus disease (COVID-2019) situation reports. (Available at).
Wikipedia: United States. Available at: https://en.wikipedia.org/wiki/United_States.
World Health Organization: Coronavirus disease (COVID-19) pandemic. Available at: https://www.who.int/emergencies/diseases/novel-coronavirus-2019.
Wu, J.-T., Leung, K., & Leung, G. M. (2020). Nowcasting and forecasting the potential domestic and international spread of the 2019-nCoV outbreak originating in Wuhan, China: A modelling study. *Lancet, 395*, 689–697.
Yang, C., & Wang, J. (2020). A mathematical model for the novel coronavirus epidemic in Wuhan, China. *Mathematical Biosciences and Engineering, 17*(3), 2708–2724.
Yang, C., Wang, X., Gao, D., & Wang, J. (2017). Impact of awareness programs on cholera dynamics: Two modeling approaches. *Bulletin of Mathematical Biology, 79*(9), 2109–2131.
Yeo, C., Kaushal, S., & Yeo, D. (2020). Enteric involvement of coronaviruses: Is faecal-oral transmission of SARS-CoV-2 possible? *The Lancet Gastroenterology and Hepatology, 5*(4), 335–337.
Zhong, H., & Wang, W. (2020). Mathematical analysis for COVID-19 resurgence in the contaminated environment. *Mathematical Biosciences and Engineering, 17*(6), 6909–6927.